

## Thermal decomposition of the Kitaev material $\alpha$ -RuCl<sub>3</sub> and its influence on low-temperature behavior

Franziska A. Breitner, Anton Jesche, Vladimir Tsurkan, Philipp Gegenwart

### Angaben zur Veröffentlichung / Publication details:

Breitner, Franziska A., Anton Jesche, Vladimir Tsurkan, and Philipp Gegenwart. 2023.  
"Thermal decomposition of the Kitaev material  $\alpha$ -RuCl<sub>3</sub> and its influence on  
low-temperature behavior." *Physical Review B* 108 (4): 045103.  
<https://doi.org/10.1103/physrevb.108.045103>.

### Nutzungsbedingungen / Terms of use:

licgercopyright

Dieses Dokument wird unter folgenden Bedingungen zur Verfügung gestellt: / This document is made available under these conditions:

**Deutsches Urheberrecht**

Weitere Informationen finden Sie unter: / For more information see:

<https://www.uni-augsburg.de/de/organisation/bibliothek/publizieren-zitieren-archivieren/publiz/>



# Thermal decomposition of the Kitaev material $\alpha$ -RuCl<sub>3</sub> and its influence on low-temperature behavior

Franziska A. Breitner,<sup>1,\*</sup> Anton Jesche,<sup>1</sup> Vladimir Tsurkan,<sup>2,3</sup> and Philipp Gegenwart<sup>1,†</sup>

<sup>1</sup>Experimental Physics VI, Center for Electronic Correlations and Magnetism, University of Augsburg, Augsburg, Germany

<sup>2</sup>Experimental Physics V, Center for Electronic Correlations and Magnetism, University of Augsburg, Augsburg, Germany

<sup>3</sup>Institute of Applied Physics, Moldova State University, Chisinau, Moldova



(Received 24 March 2023; revised 26 May 2023; accepted 21 June 2023; published 5 July 2023)

We explore the effect of heat treatment in argon atmosphere under various temperatures up to 500 °C on single crystals of  $\alpha$ -RuCl<sub>3</sub> by the study of the mass loss, microprobe energy-dispersive x-ray spectroscopy, powder x-ray diffraction, and electrical resistance, as well as low-temperature magnetic susceptibility and specific heat. Clear signatures of dechlorination and oxidation of Ru appear for annealing temperatures beyond 300 °C. Analysis of the specific heat below 2 K reveals a RuO<sub>2</sub> mass fraction of order 1% for pristine  $\alpha$ -RuCl<sub>3</sub> which increases up to 20% after thermal annealing, fully consistent with mass-loss analysis. The small RuO<sub>2</sub> inclusions drastically reduce the global electrical resistance and may thus significantly affect low-temperature thermal transport and Hall effect.

DOI: [10.1103/PhysRevB.108.045103](https://doi.org/10.1103/PhysRevB.108.045103)

## I. INTRODUCTION

The 4d layered spin-orbit Mott insulator  $\alpha$ -RuCl<sub>3</sub> [1–4] is one of the most studied “Kitaev materials” [5,6], implying nearest-neighbor bond-directional Ising interactions on the honeycomb lattice [7]. The pure Kitaev model offers an exciting route toward a quantum spin liquid with exotic fractionalized excitations and potential application for topological quantum computation [7–9]. Although  $\alpha$ -RuCl<sub>3</sub> displays a zigzag magnetic order below  $T_N \sim 7$ –8 K [10–12], its intriguing dynamical properties [4,13,14] and the possibility to suppress the order by moderate in-plane magnetic fields [11,15,16] led to a strong interest in this material. This was further boosted in 2018 when Kasahara *et al.* reported a half-integer quantized plateau in the thermal Hall conductance, in accordance with chiral Majorana edge modes [17]. Subsequent studies of the thermal Hall effect by different groups however questioned a generic regime of half quantization and indicated that the thermal Hall conductance is strongly sample dependent [18–25]. Oscillatory structures of the magnetothermal conductivity [20] were related to coexistent secondary phases that feature differing critical magnetic fields due to stacking disorder [23].  $\alpha$ -RuCl<sub>3</sub> has a monoclinic symmetry at room temperature [12,26] and displays a first-order structural transition with large hysteresis around 150 K [27,28]. Crystals with structural domains featuring stacking disorder show multiple antiferromagnetic transitions in the specific heat [12,26,28]. This holds mainly for powder specimens and low-quality crystals, whose signature in the specific heat is an anomaly near 14 K. High-quality single-crystalline samples usually show only one transition at 7 K, which can be

observed in the heat capacity as a sharp peak [29]. Stacking disorder can however easily arise in the van der Waals material  $\alpha$ -RuCl<sub>3</sub> by non-careful handling or small strain effects during cooling.

In addition, it has been known since 1968 that transition-metal chloride hydrates are chemically unstable and decompose upon heating above 150 °C [30]. This raises the question of whether a possible degradation of  $\alpha$ -RuCl<sub>3</sub> single crystals may influence its low-temperature physical properties. In particular, if  $\alpha$ -RuCl<sub>3</sub> undergoes a thermally activated degradation, then it could be assumed that already during growth some small fraction of the crystals become degraded. This motivates our systematic study of the effect of moderate temperature treatments on high-quality  $\alpha$ -RuCl<sub>3</sub> single crystals.

In this paper, we report on thermal annealing (in argon atmosphere) studies on  $\alpha$ -RuCl<sub>3</sub> single crystals at temperatures up to 500 °C. Analysis of the mass loss in combination with EDX and XRD reveals clear evidence for dechlorination and the formation of RuO<sub>2</sub> clusters penetrating from the surface into the bulk. While RuO<sub>2</sub> inclusions have little influence on magnetic susceptibility or on the specific heat anomaly at  $T_N$ , they dominate over the gapped magnon contribution in  $C(T)$  below 2 K. The low- $T$  specific heat reveals approximately 1% RuO<sub>2</sub> even in untreated  $\alpha$ -RuCl<sub>3</sub> single crystals. Our study shows that the bulk electrical conductance is strongly enhanced by metallic RuO<sub>2</sub> inclusions suggesting that the latter may also affect the low- $T$  thermal transport properties.

## II. METHODS

The initial material, commercial anhydrous RuCl<sub>3</sub> powder (Alfa Aesar), was loaded in a quartz ampoule in an Argon box with O<sub>2</sub> and H<sub>2</sub>O content below the ppm range. The ampoule was locked and transferred to the pumping system with a turbomolecular pump. A clear sign of contamination was

\*franziska.breitner@physik.uni-augsburg.de

†philipp.gegenwart@physik.uni-augsburg.de

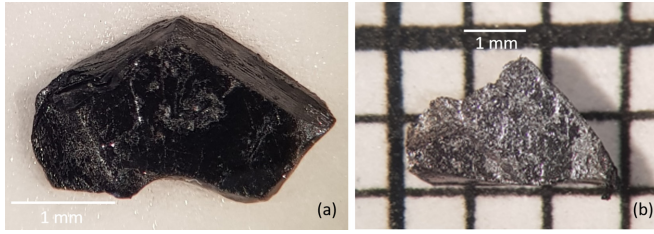


FIG. 1. Crystals used for heat capacity study. Sample 1 (a) is shown before heat treatments, sample 2 (b) after being heat treated at 500 °C in argon flow.

observed at the initial stage of the pumping by a strong decrease of the vacuum once the heating was switched on. Therefore, the ampoule was further pumped at least over 24 h under heating at 120 °C before the starting material was used for the crystal growth by vacuum sublimation [31]. The growth of the single crystals was performed in quartz ampoules evacuated to  $\sim 10^{-4}$  mbar. To reduce convection that can be a possible reason of the appearance of stacking faults the horizontal mass transport was utilized. The temperature gradient was varied between 5–10 °C for different growth runs. The ampoule was heated up to a temperature of 1000 °C, soaked for 10 h, and then slowly cooled to 600 °C with a rate of 1 °C/h. Zero-field heat capacity measurements were done to check the quality of all crystals before heat treatments. Thereby, a single transition at 7 K and no signature at 14 K were detected.

Heat treatments were performed in two different ways; see the Supplemental Material (SM) for a table with all studied samples [32]. Two of the crystals (sample 1 and sample 5) were sealed in a quartz ampoule under 150 mbar Ar atmosphere, after evacuating the tube several times down to  $2 \times 10^{-2}$  mbar and flushing with Ar gas, then heated in a muffle furnace up to 400 or 450 °C for 12 h. To avoid contamination of the sample the quartz tube was previously cleaned using acetone and then baked out at 70 °C for one hour before inserting the crystal. The other samples were heat treated using an Al<sub>2</sub>O<sub>3</sub> crucible placed inside a differential thermal analysis (DTA) chamber, which was then evacuated down to 3 mbar and flooded with argon gas before heating the sample in Ar flow to 500 °C for 1 h. Figure 1 displays in panel (a) a photo of sample 1 before the heat treatments, with surface imperfections arising from the cleaving. Panel (b) displays the much rougher surface of a heat-treated sample.

Heat capacity (HC) measurements in the range of 0.35–20 K were performed in a Quantum Design PPMS with the helium-3 option. The samples were mounted onto the platform using Apiezon N grease. Magnetic susceptibility in the range of 2–300 K was measured utilizing the Quantum Design MPMS 3. The sample was mounted onto a quartz rod using GE varnish and later removed using isopropanol. Electrical transport measurements in the range of 125–300 K were performed in the PPMS utilizing the ETO option. Contacts for four-wire measurements were made using two-component silver epoxy.

Powder x-ray diffraction measurements were performed using a Rigaku Miniflex600 powder diffractometer (Cu-K $\alpha$  radiation). A scanning electron microscope (SEM; Merlin

TABLE I. Comparison of the masses of RuO<sub>2</sub> in the initial and heat-treated samples determined via fit to the low-*T* heat capacity versus values calculated from mass loss determined by balance. The error for the relative RuO<sub>2</sub> mass ratio determined from HC amounts to 0.2% for the pristine samples and is even smaller for the annealed crystals.

	$m_{\text{sample}}$	$m_{\text{RuO}_2, \text{balance}}$	$m_{\text{RuO}_2, \text{HC}}$	$\frac{m_{\text{RuO}_2, \text{HC}}}{m_{\text{sample}}}$
Sample 1	6.34(2) mg		0.06(1) mg	0.9(2)%
400 °C	5.96(3) mg	0.68(12) mg	0.61(2) mg	10.2%
450 °C	5.84(4) mg	0.89(14) mg	0.93(4) mg	15.9%
Sample 2	5.44(2) mg		0.09(2) mg	1.6(2)%
500 °C	4.58(3) mg	0.89(10) mg	0.85(3) mg	18.6%

Gemini 2, Zeiss) equipped with an energy-dispersive x-ray (EDX) analysis probe (X-Max 80N SDD detector, Oxford Instruments) was utilized for structural and compositional investigation. Silver epoxy was used to mount the crystals onto the sample holder.

After each measurement the samples were carefully cleaned using *n*-butyl acetate to avoid carrying any epoxy or grease residue into the next measurement while at the same time avoiding damage to the crystals.

### III. RESULTS AND DISCUSSION

Before performing any kind of heat treatments we checked whether the specific heat is affected by multiple removals from HC and EDX pucks as it is known that less careful handling can potentially induce stacking disorder that profoundly changes the  $T_N$  and the signature of magnetic order [12]. As shown in the SM [32], no change in the HC was found, confirming that any changes in our study are induced by heat treatments.

For sample 1, heat treatments were performed at increasing temperatures, until a change in the HC could be detected. The first change was observed after heat treatment at 400 °C. Already an increase of the HC toward low temperatures for temperatures below 1.5 K as well as a shrinking of the peak at 7 K can be detected, as can be seen in Fig. 2(a). The procedure was repeated with a maximum heat treatment temperature of 450 °C. Again, the HC showed an even more pronounced increase toward low temperatures. Here, the exponential impact of the maximum temperature on the activation process exceeds that of longer dwell time, and thus no experiments with longer dwell times were conducted.

After each step the sample mass was determined. Each heat treatment led to a notable decrease, the exact values of which are listed in Table I.

The heat treatment for sample 2 was performed at 500 °C in argon flow. Comparing the HC of the heat-treated and the untreated crystal, as shown in Fig. 2(b), the same increase toward low temperatures and shrinking of the 7 K peak can be observed.

Compared to its initial mass of 5.44 mg the mass of the heat-treated sample 2 was reduced to 4.58 mg indicating a relative mass loss of 16%. As the sample surface appeared rather porous after heat treatment, very careful handling

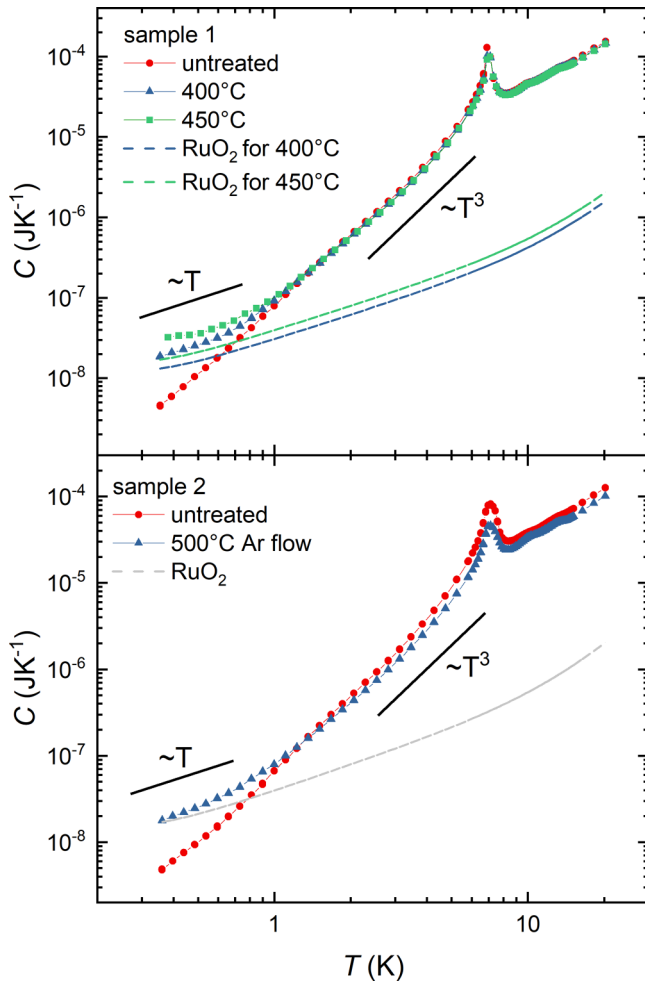


FIG. 2. Heat capacity of initial samples 1 and 2 compared with those after several heat treatments. For  $T < 1.5$  K the heat capacity increases toward low temperatures with increasing annealing temperature, while the peak at 7 K is reduced by magnitude. For comparison, the fraction of heat capacity attributed to  $\text{RuO}_2$  is shown as dotted lines.

was required to avoid parts breaking off during transport or handling.

EDX was used to determine the sample stoichiometry and map the elemental distribution on the surface. After the initial consistency check, EDX analysis was only performed once the HC changed in order to minimize stress on the crystal. For the untreated crystals, the obtained molar ratio of Ru:Cl amounted to 25(3):75(3); both Ru and Cl were evenly distributed across the observed surface, as can be seen in the SM [32]. No significant change in elemental distribution was observed for temperatures up to 300 °C. However, it should be noted that only a fraction of the crystal surface was evaluated in greater detail due to spatial limitations and time constraints. Upon heating sample 1 to 400 °C, the formation of clusters, some as large as 70  $\mu\text{m}$  in diameter, was observed [see Figs. 3(a)–3(c)]. Stoichiometry analysis of such clusters shows a decrease of Cl concentration down to 25 at. % in some areas and a corresponding increase in Ru concentration. Averaging over the investigated surface, the molar ratio of Ru:Cl is determined to be about 30:70 for sample 1 treated at 400 °C and 32:68 for 450 °C. We therefore conclude that further degradation of the sample has occurred due to the second heat treatment.

After heat treatment at 500 °C sample 2 did not show any visible formation of clusters; however the Cl concentration was significantly diminished across the whole crystal surface. The average molar ratio Ru:Cl was determined to be 62:38.

As EDX analysis is limited to the surface layers due to a penetration depth of the electron beam below  $\sim 1$   $\mu\text{m}$ , the question arises as to how deep into the crystal this effect can still be observed. For this purpose, another crystal (sample 3) was prepared as previously described in order to investigate the penetration depth of the degradation process without rendering sample 2 unusable for further measurements. From sample 3 a few layers were peeled off, and then the crystal was cut into half and EDX was performed on the freshly obtained surfaces. The distribution of Ru and Cl on the surface can be seen in Fig. 3(d), revealing large areas on the crystal surface

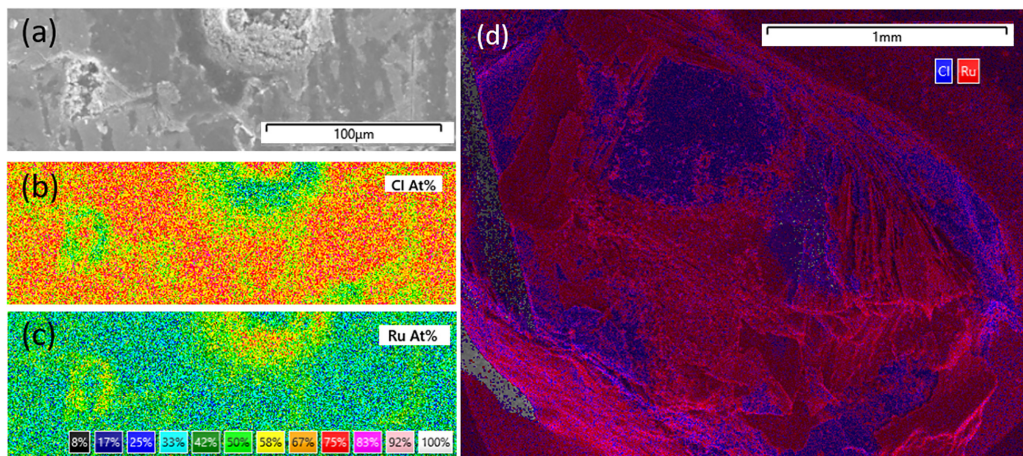


FIG. 3. Elemental maps of Ru and Cl for sample 1 after heat treatment at 400 °C [(a)–(c)] and sample 3 which was treated analogously to sample 2 (d). For sample 1 in some areas a significant increase in the Ru concentration along with a corresponding decrease in the Cl concentration can be observed [e.g., green areas in (b)]. Sample 3 displays an overall diminished Cl concentration on the surface, with large parts of the surface showing a majority of Ru.



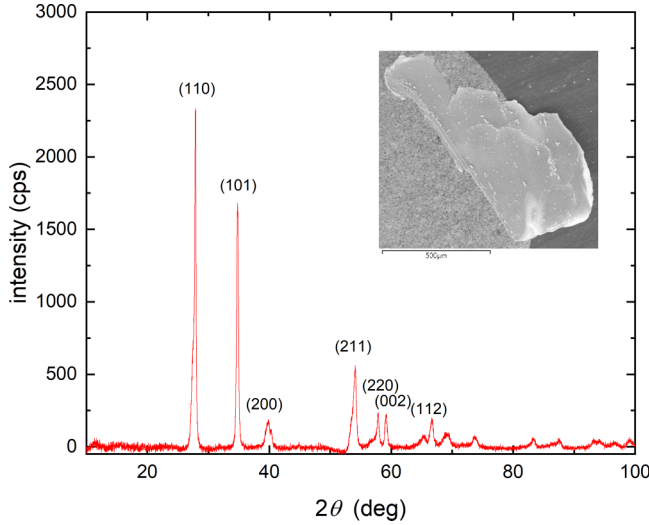


FIG. 4. XRD pattern of ground surface material. The peaks match those for  $\text{RuO}_2$ . The inset shows the surface flake retrieved from a heat-treated crystal which was ground and used for the XRD measurement.

with predominantly Ru being detected. While after a few layers, the molar ratio of Ru:Cl is still significantly enhanced to 44:56, roughly halfway into the 0.5 mm thick crystal only 27 at. % Ru is detected. In order to determine whether the accumulated Ru on the surface is metallic ruthenium or some other product, enough material was carefully removed from the crystal surface and ground into fine powder using an agate mortar and pestle in order to perform x-ray powder diffraction. The obtained diffraction pattern shown in Fig. 4 matches that of the metallic transition-metal oxide  $\text{RuO}_2$  [33] while no pure Ru could be detected.

Using this information we examine the low- $T$  HC of initial and heat-treated  $\alpha\text{-RuCl}_3$  for samples 1 and 2. As shown in Fig. 5, the measured data below 1.9 K are described by the sum of two contributions arising from phonons in  $\alpha\text{-RuCl}_3$  and phonons and electrons in  $\text{RuO}_2$ . Note that the magnon contribution  $\sim \exp(-\Delta/k_B T)$  with  $\Delta = 1.7$  meV [15] is negligible compared to phonons in this temperature range. For the fit, we used the measured total sample mass and described the total HC (in units of J/K) by the function  $C/T = (m_{\text{sample}} - m_{\text{RuO}_2, \text{HC}})(\beta_{\text{RuCl}_3} T^2) + m_{\text{RuO}_2, \text{HC}} C_{\text{m, RuO}_2} / T$  with  $m_{\text{RuO}_2, \text{HC}}$  as the free fit parameter. The (molar) specific heat of  $\text{RuO}_2$  was measured on a pellet and found to be in good agreement with the literature [34]. For details, we refer to the SM [32]. The converted (mass) specific heat  $C_{\text{m, RuO}_2}$  was then used in the above fit of the HC. The fit also includes the phonon contribution of  $\beta_{\text{RuCl}_3}$ , which was determined by fitting the untreated crystals (yielding the parameters given in the caption of Fig. 5) and then fixed for all further fits. The fitted values for  $m_{\text{RuO}_2, \text{HC}}$  listed in Table I are in good agreement with those obtained from the analysis of the weight loss according to  $m_{\text{RuO}_2, \text{scale}} = \Delta m (1 - \frac{M_{\text{RuCl}_3}}{M_{\text{RuO}_2}})^{-1}$ , where  $\Delta m < 0$  denotes the measured mass difference between heat-treated and pristine samples, arising by the loss of chlorine and gain of oxygen according to  $2\text{RuCl}_3 + 2\text{O}_2 \rightarrow 2\text{RuO}_2 + 3\text{Cl}_2$ . Applying the same fitting procedure to the HC of the pristine samples yields

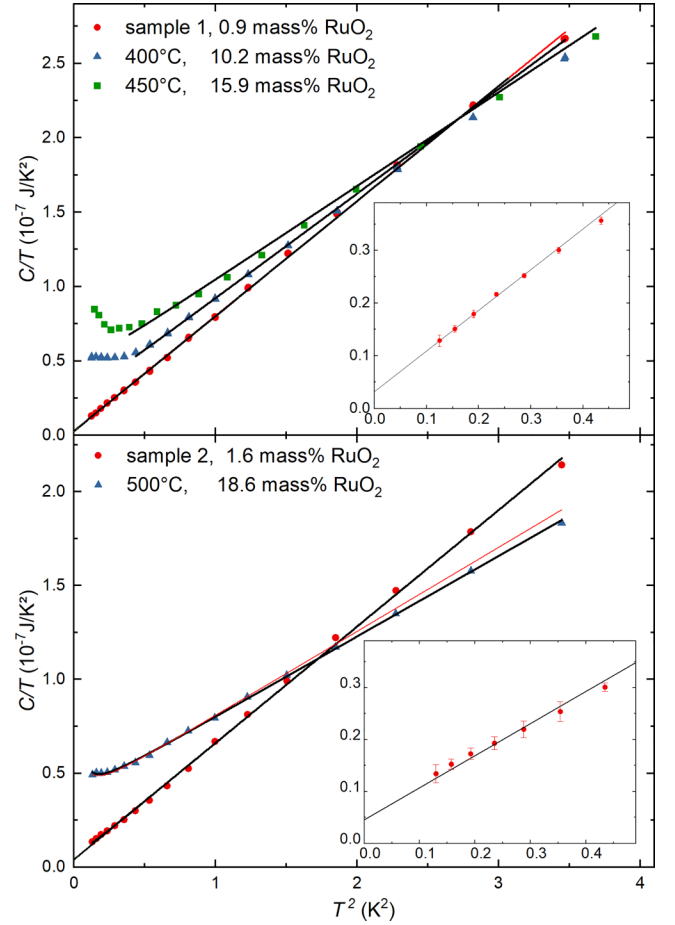


FIG. 5. Heat capacity as  $C/T$  vs  $T^2$  for sample 1 (upper) and 2 (lower panel) before (red circles) and after (blue triangles) heat treatments. The black solid lines are fits according  $C/T = (m_{\text{sample}} - m_{\text{RuO}_2, \text{HC}})(\beta_{\text{RuCl}_3} T^2) + m_{\text{RuO}_2, \text{HC}} C_{\text{m, RuO}_2} / T$  with masses as listed in Table I,  $\beta_{\text{RuCl}_3} = 1.29$  and  $1.18 \times 10^{-5} \text{ J/g K}^4$  for sample 1 and 2, respectively. The heat capacity of  $\text{RuO}_2$  is described by  $C_{\text{m, RuO}_2} = M_{\text{RuO}_2}^{-1} (\alpha T^{-2} + \beta T^3 + \gamma T)$  with  $\alpha = 5.9 \times 10^{-5} \text{ J K/mol}$ ,  $\beta = 2.25 \times 10^{-5} \text{ J/mol K}^4$ , and  $\gamma = 5.77 \times 10^{-3} \text{ J/mol K}^2$  [32].

$\text{RuO}_2$  masses corresponding to 1%–2% of total sample mass. This suggests that even in unannealed crystals of  $\text{RuCl}_3$  a tiny  $\text{RuO}_2$  metal fraction cannot be excluded. Furthermore, the Sommerfeld coefficient of the respective  $\text{RuO}_2$  contribution can be accessed directly by looking at the intersection of the fit function with the  $C/T$  axis; cf. the insets of Fig. 5.

Fitting with the heat capacity with Ru instead of  $\text{RuO}_2$  yields fits of lower quality with Ru masses significantly higher than what would be possible due to the measured mass loss. Another possibility would be to fit the data with a combination of Ru and  $\text{RuO}_2$ . However, fitting with the masses as free parameters results in the same values as obtained for the fit with just  $\text{RuO}_2$  and the mass of Ru chosen as zero. We therefore conclude that most if not all of the degraded  $\alpha\text{-RuCl}_3$  turns into  $\text{RuO}_2$  upon heating.

Another crystal (sample 4) was used to investigate the change in magnetic behavior due to heat treatment. The sample was tempered at  $500^\circ\text{C}$  in argon flow for 1 h analogous to sample 2. The susceptibility measurement of the heat-treated

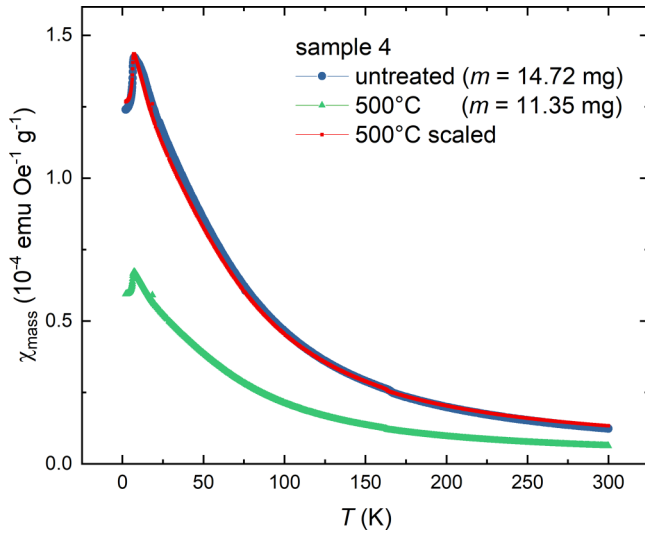


FIG. 6. Temperature dependence of the magnetic susceptibility measured with a magnetic field of  $H = 1$  T applied along the  $ab$  plane before and after heat treatment at  $500^\circ\text{C}$ . The values given in parentheses refer to the sample masses, wherein the heat-treated sample contains 6 mg  $\text{RuO}_2$  according to calculation from mass loss. Scaling the heat-treated measurement (green) with a corrected mass of  $\alpha\text{-RuCl}_3$  due to degradation yields a plot (red) corresponding to that of the initial sample (blue).

crystal showed significantly lower absolute values compared to the initial measurement (see Fig. 6). Scaling with the  $\alpha\text{-RuCl}_3$  and  $\text{RuO}_2$  concentration determined from mass loss resulted in a plot showing good agreement with the first measurement.

Electrical transport measurements were performed on a pristine and  $400^\circ\text{C}$  heat-treated crystal (sample 5). While the untreated sample clearly shows insulating behavior, the resistivity of the heat-treated sample changes by several orders of magnitude (see Fig. 7). From previous analysis, we know that after heat treatment at  $400^\circ\text{C}$  only  $\sim 10\%$  of the sample consists of  $\text{RuO}_2$  resulting in a deviation visible only at very low temperatures in heat capacity, yet the influence on the electronic transport properties is significant over the whole temperature range. For comparison we also plotted the resistivity of pure  $\text{RuO}_2$  [35], revealing that the values of the heat-treated sample are already closer to that of  $\text{RuO}_2$  than  $\alpha\text{-RuCl}_3$ . Since millikelvin thermal conductance of metallic  $\text{RuO}_2$  is far higher than that of insulating  $\alpha\text{-RuCl}_3$ , we expect a significant influence of  $\text{RuO}_2$  inclusions on the low- $T$  thermal transport and Hall effect.

Remarkably we find a complete oxidation of dechlorinated ruthenium in our experiments, despite sealing the samples in an ampoule which was evacuated and flushed with argon gas several times. In air  $\alpha\text{-RuCl}_3$  is extremely sensitive to decomposition and oxidation already under very moderate heating [30]. While it is well established that  $\alpha\text{-RuCl}_3$  needs to be handled mechanically with maximal care to avoid the formation of stacking faults, our experiments indicate that in addition special care is needed to avoid degradation and oxidation. This concerns for instance long-term storage in air or baking of glued metal wire contacts on the crystal surface, required for thermal transport measurements. Protected gas

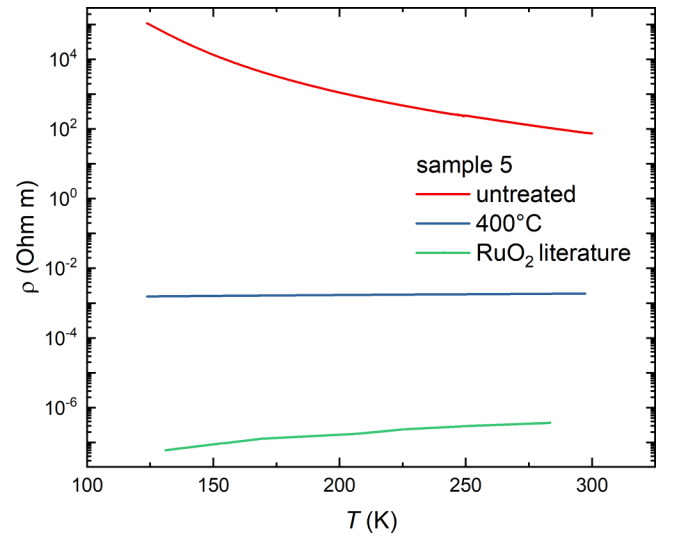


FIG. 7. Measurement of the electrical transport in the temperature range of 125–300 K for an untreated (red) and heat-treated at  $400^\circ\text{C}$  (blue)  $\alpha\text{-RuCl}_3$  crystal. The green line shows literature data [35] of pure  $\text{RuO}_2$ .

atmosphere is recommended, along with careful check for partial dechlorination and oxidation.

It should further be noted that XRD analysis of a different batch revealed the as purchased powder to not be pure  $\alpha\text{-RuCl}_3$ , but rather containing some  $\text{RuO}_2$  and other impurities. This would offer a possible explanation for the small (of order 1%)  $\text{RuO}_2$  fraction in the initial crystals, yet not for the increase in  $\text{RuO}_2$  for annealed crystals. While the exact origin of oxygen for the degradation reaction in our study remains unclear [32], the above mentioned observations along with the heat capacity data lead us to conclude that even for unannealed crystals the presence of a small percentage of metallic  $\text{RuO}_2$  cannot be excluded.

#### IV. CONCLUSION

In conclusion, we performed heat treatments on  $\alpha\text{-RuCl}_3$  single crystals in closed argon atmosphere up to  $450^\circ\text{C}$  as well as argon flow up to  $500^\circ\text{C}$  in order to investigate the impact of annealing on the low-temperature physical properties. Both samples showed enhanced heat capacity toward low temperatures for  $T < 1.5$  K. SEM and EDX revealed the formation of Ru-rich clusters on the surface of sample 1 and an overall decreased percentage of Cl on the surface of sample 2, after the samples were heated to at least  $400^\circ\text{C}$ . Dechlorination and oxidation takes place beneath the sample surface to some degree; however, this seems to be less pronounced toward the center of the investigated crystal. Powder XRD analysis revealed the surface material to be  $\text{RuO}_2$ . The deviation of both heat capacity and susceptibility measured after heat treatment from the initial measurement can be explained by a decreased amount of  $\alpha\text{-RuCl}_3$  along with the formation of  $\text{RuO}_2$ . The  $\text{RuO}_2$  content determined via fit in both cases agrees well with the value calculated from the measured mass loss and amounts to 10–20 mass %. Such relatively small mass fraction of metallic  $\text{RuO}_2$  already reduces

the electrical resistance of degraded  $\alpha$ -RuCl<sub>3</sub> by several orders of magnitude. Importantly, the low-temperature specific-heat analysis of pristine  $\alpha$ -RuCl<sub>3</sub> crystals (before thermal treatment) also yields the presence of 0.9–1.6 mass % RuO<sub>2</sub>. It would be important to clarify whether such a low fraction of metallic inclusions as found in pristine crystals, though effectively invisible in most physical properties, may have an impact on the low-temperature thermal transport and Hall effect in  $\alpha$ -RuCl<sub>3</sub> crystals, as found in our electrical transport measurements.

## ACKNOWLEDGMENTS

We are grateful to Alexander Herrnberger and Klaus Wiedenmann for technical support and acknowledge fruitful discussions with Alexander A. Tsirlin, A. Loidl, Y.-J. Kim, S. E. Nagler, and R. Valenti. This work was supported by the German Research Foundation through TRR80 (Project No. 107745057). Partial support of the National Agency for Research and Development of Moldova (NARD) via Project No. 20.80009.5007.19 is acknowledged.

- [1] K. Plumb, J. Clancy, L. Sandilands, V. V. Shankar, Y. Hu, K. Burch, H.-Y. Kee, and Y.-J. Kim,  $\alpha$ -RuCl<sub>3</sub>: A spin-orbit assisted Mott insulator on a honeycomb lattice, *Phys. Rev. B* **90**, 041112(R) (2014).
- [2] L. J. Sandilands, Y. Tian, A. A. Reijnders, H.-S. Kim, K. W. Plumb, Y.-J. Kim, H.-Y. Kee, and K. S. Burch, Spin-orbit excitations and electronic structure of the putative Kitaev magnet  $\alpha$ -RuCl<sub>3</sub>, *Phys. Rev. B* **93**, 075144 (2016).
- [3] S. Agrestini, C.-Y. Kuo, K.-T. Ko, Z. Hu, D. Kasinathan, H. B. Vasili, J. Herrero-Martin, S. Valvidares, E. Pellegrin, L.-Y. Jang *et al.*, Electronically highly cubic conditions for Ru in  $\alpha$ -RuCl<sub>3</sub>, *Phys. Rev. B* **96**, 161107(R) (2017).
- [4] A. Banerjee, C. Bridges, J.-Q. Yan, A. Aczel, L. Li, M. Stone, G. Granroth, M. Lumsden, Y. Yiu, J. Knolle *et al.*, Proximate Kitaev quantum spin liquid behaviour in a honeycomb magnet, *Nat. Mater.* **15**, 733 (2016).
- [5] S. M. Winter, A. A. Tsirlin, M. Daghofer, J. van den Brink, Y. Singh, P. Gegenwart, and R. Valenti, Models and materials for generalized Kitaev magnetism, *J. Phys.: Condens. Matter* **29**, 493002 (2017).
- [6] H. Takagi, T. Takayama, G. Jackeli, G. Khaliullin, and S. E. Nagler, Concept and realization of Kitaev quantum spin liquids, *Nat. Rev. Phys.* **1**, 264 (2019).
- [7] A. Kitaev, Anyons in an exactly solved model and beyond, *Ann. Phys.* **321**, 2 (2006).
- [8] A. Y. Kitaev, Fault-tolerant quantum computation by anyons, *Ann. Phys.* **303**, 2 (2003).
- [9] M. Hermanns, I. Kimchi, and J. Knolle, Physics of the Kitaev model: Fractionalization, dynamic correlations, and material connections, *Annu. Rev. Condens. Matter Phys.* **9**, 17 (2018).
- [10] J. A. Sears, M. Songvilay, K. Plumb, J. Clancy, Y. Qiu, Y. Zhao, D. Parshall, and Y.-J. Kim, Magnetic order in  $\alpha$ -RuCl<sub>3</sub>: A honeycomb-lattice quantum magnet with strong spin-orbit coupling, *Phys. Rev. B* **91**, 144420 (2015).
- [11] J. A. Sears, Y. Zhao, Z. Xu, J. W. Lynn, and Y.-J. Kim, Phase diagram of  $\alpha$ -RuCl<sub>3</sub> in an in-plane magnetic field, *Phys. Rev. B* **95**, 180411(R) (2017).
- [12] H. B. Cao, A. Banerjee, J.-Q. Yan, C. A. Bridges, M. D. Lumsden, D. G. Mandrus, D. A. Tennant, B. C. Chakoumakos, and S. E. Nagler, Low-temperature crystal and magnetic structure of  $\alpha$ -RuCl<sub>3</sub>, *Phys. Rev. B* **93**, 134423 (2016).
- [13] L. J. Sandilands, Y. Tian, K. W. Plumb, Y.-J. Kim, and K. S. Burch, Scattering Continuum and Possible Fractionalized Excitations in  $\alpha$ -RuCl<sub>3</sub>, *Phys. Rev. Lett.* **114**, 147201 (2015).
- [14] H.-S. Kim, Vijay Shankar V., A. Catuneanu, and H.-Y. Kee, Kitaev magnetism in honeycomb RuCl<sub>3</sub> with intermediate spin-orbit coupling, *Phys. Rev. B* **91**, 241110(R) (2015).
- [15] A. Banerjee, P. Lampen-Kelley, J. Knolle, C. Balz, A. A. Aczel, B. Winn, Y. Liu, D. Pajerowski, J. Yan, C. A. Bridges *et al.*, Excitations in the field-induced quantum spin liquid state of  $\alpha$ -RuCl<sub>3</sub>, *npj Quantum Mater.* **3**, 8 (2018).
- [16] S.-H. Baek, S.-H. Do, K.-Y. Choi, Y. S. Kwon, A. Wolter, S. Nishimoto, J. van den Brink, and B. Büchner, Evidence for a Field-Induced Quantum Spin Liquid in  $\alpha$ -RuCl<sub>3</sub>, *Phys. Rev. Lett.* **119**, 037201 (2017).
- [17] Y. Kasahara, T. Ohnishi, Y. Mizukami, O. Tanaka, S. Ma, K. Sugii, N. Kurita, H. Tanaka, J. Nasu, Y. Motome, T. Shibauchi, and Y. Matsuda, Majorana quantization and half-integer thermal quantum Hall effect in a Kitaev spin liquid, *Nature (London)* **559**, 227 (2018).
- [18] M. Yamashita, J. Gouchi, Y. Uwatoko, N. Kurita, and H. Tanaka, Sample dependence of half-integer quantized thermal Hall effect in the Kitaev spin-liquid candidate  $\alpha$ -RuCl<sub>3</sub>, *Phys. Rev. B* **102**, 220404(R) (2020).
- [19] T. Yokoi, S. Ma, Y. Kasahara, S. Kasahara, T. Shibauchi, N. Kurita, H. Tanaka, J. Nasu, Y. Motome, C. Hickey, S. Trebst, and Y. Matsuda, Half-integer quantized anomalous thermal Hall effect in the Kitaev material candidate  $\alpha$ -RuCl<sub>3</sub>, *Science* **373**, 568 (2021).
- [20] P. Czajka, T. Gao, M. Hirschberger, P. Lampen-Kelley, A. Banerjee, J. Yan, D. G. Mandrus, S. E. Nagler, and N. Ong, Oscillations of the thermal conductivity in the spin-liquid state of  $\alpha$ -RuCl<sub>3</sub>, *Nat. Phys.* **17**, 915 (2021).
- [21] J. Bruin, R. Claus, Y. Matsumoto, N. Kurita, H. Tanaka, and H. Takagi, Robustness of the thermal Hall effect close to half-quantization in  $\alpha$ -RuCl<sub>3</sub>, *Nat. Phys.* **18**, 401 (2022).
- [22] É. Lefrançois, G. Grissonnanche, J. Baglo, P. Lampen-Kelley, J.-Q. Yan, C. Balz, D. Mandrus, S. Nagler, S. Kim, Y.-J. Kim, N. Doiron-Leyraud, and L. Taillefer, Evidence of a Phonon Hall Effect in the Kitaev Spin Liquid Candidate  $\alpha$ -RuCl<sub>3</sub>, *Phys. Rev. X* **12**, 021025 (2022).
- [23] J. A. N. Bruin, R. R. Claus, Y. Matsumoto, J. Nuss, S. Laha, B. V. Lotsch, N. Kurita, H. Tanaka, and H. Takagi, Origin of oscillatory structures in the magnetothermal conductivity of the putative Kitaev magnet  $\alpha$ -RuCl<sub>3</sub>, *APL Mater.* **10**, 090703 (2022).
- [24] P. Czajka, T. Gao, M. Hirschberger, P. Lampen-Kelley, A. Banerjee, N. Quirk, D. G. Mandrus, S. E. Nagler, and N. Ong, The planar thermal Hall conductivity in the Kitaev magnet  $\alpha$ -RuCl<sub>3</sub>, *Nat. Mater.* **22**, 36 (2023).
- [25] H. Zhang, A. F. May, H. Miao, B. C. Sales, D. G. Mandrus, S. E. Nagler, M. A. McGuire, and J. Yan, The sample-dependent and sample-independent thermal transport properties of  $\alpha$ -RuCl<sub>3</sub>, *arXiv:2303.02098*.

- [26] R. D. Johnson, S. Williams, A. Haghighirad, J. Singleton, V. Zapf, P. Manuel, I. Mazin, Y. Li, H. O. Jeschke, R. Valentí *et al.*, Monoclinic crystal structure of  $\alpha$ -RuCl<sub>3</sub> and the zigzag antiferromagnetic ground state, *Phys. Rev. B* **92**, 235119 (2015).
- [27] S. Gass, P. M. Consoli, V. Kocsis, L. T. Corredor, P. Lampen-Kelley, D. G. Mandrus, S. E. Nagler, L. Janssen, M. Vojta, B. Buchner, and A. U. B. Wolter, Field-induced transitions in the Kitaev material  $\alpha$ -RuCl<sub>3</sub> probed by thermal expansion and magnetostriction, *Phys. Rev. B* **101**, 245158 (2020).
- [28] Y. Kubota, H. Tanaka, T. Ono, Y. Narumi, and K. Kindo, Successive magnetic phase transitions in  $\alpha$ -RuCl<sub>3</sub>: XY-like frustrated magnet on the honeycomb lattice, *Phys. Rev. B* **91**, 094422 (2015).
- [29] A. Banerjee, J. Yan, J. Knolle, C. A. Bridges, M. B. Stone, M. D. Lumsden, D. G. Mandrus, D. A. Tennant, R. Moessner, and S. E. Nagler, Neutron scattering in the proximate quantum spin liquid  $\alpha$ -RuCl<sub>3</sub>, *Science* **356**, 1055 (2017).
- [30] A. Newkirk and D. McKee, Thermal decomposition of rhodium, iridium and ruthenium chlorides, *J. Catal.* **11**, 370 (1968).
- [31] S. Reschke, F. Mayr, S. Widmann, H.-A. K. Von Nidda, V. Tsurkan, M. V. Eremin, S.-H. Do, K.-Y. Choi, Z. Wang, and A. Loidl, Sub-gap optical response in the Kitaev spin-liquid candidate  $\alpha$ -RuCl<sub>3</sub>, *J. Phys.: Condens. Matter* **30**, 475604 (2018).
- [32] See Supplemental Material at <http://link.aps.org/supplemental/10.1103/PhysRevB.108.045103> including specific heat of untreated samples, the effect of heat treatment on the  $T_N$  signature in heat capacity, energy-dispersive x-ray spectroscopy results of a heat-treated sample, specific heat of RuO<sub>2</sub>, and a discussion on oxidation upon heating in argon atmosphere.
- [33] M. Khachane, P. Nowakowski, S. Villain, J. Gavarri, C. Muller, I. Luk'Yanchuk, M. Elaatmani, A. Outzourhit, and A. Zegzouti, Catalytic studies of RuO<sub>2</sub> films deposited on ferroelectrics films by spin coating process, *Ferroelectrics* **371**, 34 (2008).
- [34] B. Passenheim and D. McCollum, Heat capacity of RuO<sub>2</sub> and IrO<sub>2</sub> between 0.54 and 10 K, *J. Chem. Phys.* **51**, 320 (1969).
- [35] S. Butler and J. Gillson, Crystal growth, electrical resistivity and lattice parameters of RuO<sub>2</sub> and IrO<sub>2</sub>, *Mater. Res. Bull.* **6**, 81 (1971).